Singlet oxygen-based photoelectrochemical detection of single-point mutations in the KRAS oncogene

Singlet oxygen-based photoelectrochemical detection of single-point mutations in the *KRAS* oncogene

Elise Daems[a,b,1], Simone Bassini[a,b,1], Laura Mariën[c,d], Hannah Op de Beeck[a,b], Alexandr Stratulat[a,b], Karen Zwaenepoel[d,e], Timon Vandamme[d,f], Ken Op de Beeck[c,d], Senada Koljenovic[d,e], Marc Peeters[d,f], Guy Van Camp[c,d], Karolien De Wael[a,b]*

[a]A-Sense Lab, Department of Bioscience Engineering, University of Antwerp, Antwerp, 2020, Belgium.

[b]NANOlab Center of Excellence, University of Antwerp, Antwerp, 2020, Belgium

[c]Center of Medical Genetics, University of Antwerp and Antwerp University Hospital, Edegem, 2650, Belgium

[d]Center for Oncological Research, Integrated Personalized & Precision Oncology Network (IPPON), University of Antwerp, Wilrijk, 2610, Belgium

[e]Department of Pathology, Antwerp University Hospital, Edegem, 2650, Belgium

[f]Department of Oncology and Multidisciplinary Oncological Center Antwerp (MOCA), Antwerp University Hospital, Edegem, 2650, Belgium

[1]These authors contributed equally to this work.

* To whom correspondence should be addressed. Email: karolien.dewael@uantwerpen.be; Phone number: +3232653335

ABSTRACT

Single nucleotide point mutations in the *KRAS* oncogene occur frequently in human cancers, rendering them intriguing targets for diagnosis, early detection and personalized treatment. Current detection methods are based on polymerase chain reaction, sometimes combined with next-generation sequencing, which can be expensive, complex and have limited availability. Here, we propose a novel singlet oxygen ($^1O_2$)-based photoelectrochemical detection methodology for single-point mutations, using *KRAS* mutations as a case study. This detection method combines the use of a sandwich assay, magnetic beads and robust chemical photosensitizers, that need only air and light to produce $^1O_2$, to ensure high specificity and sensitivity. We demonstrate that hybridization of the sandwich hybrid at high temperatures enables discrimination between mutated and wild-type sequences with a detection rate of up to 93.9%. Additionally, the presence of background DNA sequences derived from human cell-line DNA, not containing the mutation of interest, did not result in a signal, highlighting the specificity of the methodology. A limit of detection as low as 112 pM (1.25 ng/mL) was achieved without employing any amplification techniques. The developed $^1O_2$-based

photoelectrochemical methodology exhibits unique features, including rapidity, ease of use, and affordability, highlighting its immense potential in the field of nucleic acid-based diagnostics.

KEYWORDS

Photoelectrochemistry, Singlet oxygen, Nucleic acids, Single-point mutations, *KRAS* mutations

1. INTRODUCTION

Cancer refers to a disease characterized by the uncontrollable growth and spread of abnormal body cells, affecting adjacent tissue and even distant organs (Weinberg, 1996). According to the World Health Organization (WHO), cancer is the second leading cause of death worldwide, accounting for 10.0 million deaths and 19.3 million new diagnoses in 2020 (Global Cancer Observatory, 2020). Carcinogenesis is primarily linked to changes in the (epi)genome rendering molecular biomarker testing for diagnostic purposes and the precise tailoring of therapies to individual patients crucial (Sholl and Halmos, 2022; Weinberg, 1996). A well-known type of molecular biomarkers are those based on genomic mutations. A good example is mutations that occur in the *KRAS* (v-Ki-Ras2 Kirsten rat sarcoma) oncogene as these are frequently found in human tumors, including colorectal cancer (CRC), pancreatic ductal adenocarcinoma (PDAC) and non-small cell lung cancer (NSCLC) (Vacante et al., 2018). An average of 45% of all metastatic CRC, 85% of PDAC and 33% of NSCLC tumors harbor mutations in exon 2 (codons 12 and 13), 3 (codons 59 and 61) and 4 (codons 117 and 146) of the *KRAS* oncogene, making it a highly interesting target for diagnosis and early detection. In addition, *KRAS* mutations render metastatic CRC patients ineligible for epidermal growth factor receptor (EGFR) antibody therapy and thus have therapeutic implications. Finally, specific *KRAS* mutation-targeting drugs are currently in clinical development for CRC, PDAC, NSCLC and other tumor types (Hong et al., 2020).

Well-known methods for the detection of genomic mutations are DNA next-generation sequencing (NGS), quantitative polymerase chain reaction (qPCR), and digital droplet PCR (ddPCR). Moreover, fully automated but closed systems for PCR-based molecular testing, such as Idylla (BioCartis), recently entered the market. These established technologies have a high sensitivity and specificity, but come with significant challenges: relatively long time to

result, complexity, requiring specialist knowledge, low miniaturization potential, and high costs (device and consumables) causing limited accessibility (Table 1).

Table 1. Specifications of gold standard techniques for genomic mutation analysis.

Feature	Targeted NGS	qPCR	ddPCR	Idylla
Sensitivity	High	High	Very high	High
Specificity	Very high	Very high	Very high	Very high
Time to result	Long	Short	Short	Very short
Sample preparation	Complex	Simple	Simple	Very simple
Miniaturization potential	Low	Low	Low	High
Cost device (€)	250k–1m	30k–50k	50k–100k	25k–35k
Cost consumables / marker	€	€€€	€€€	€€€€
Cost of labor	High	High	High	Low

Electrochemical platforms could overcome these drawbacks since they offer advantages such as simplicity and rapid response times whilst enabling incorporation into robust, portable, low-cost, miniaturized devices that can be tailored for specific applications (Heller and Feldman, 2008; Kimmel et al., 2012; Ondraskova et al., 2023). The literature describes various electrochemical strategies for the detection of molecular cancer mutations, including several methods specifically designed for detecting *KRAS* mutations (Ondraskova et al., 2023). Numerous of these electrochemical biosensing strategies require enzymes prior to the analysis (i.e. during target amplification by PCR(Attoye et al., 2021, 2020)) or during the analysis itself (Lee et al., 2022; Wang et al., 2018; Zeng and Xiang, 2019; Zhou et al., 2020). However, a few non-enzymatic approaches were described which are summarized in Supplementary Table 1. First, Das et al. developed an approach to detect several *KRAS* mutations using a microfabricated sensing chip (Das et al., 2015). The sensor is modified with PNA probes that hybridize with the target sequences of interest. Afterwards, the signal of an electrocatalytic reporter system (i.e. $Ru(NH_3)_6^{3+}$ and $Fe(CN)_6^{3-}$) is monitored by differential pulse voltammetry to verify if the target DNA is present. Second, Yuanfeng et al. detected the *KRAS* p.G12A mutation using a gold nanocrystal-multiple graphene aerogel and a double amplification strategy (Yuanfeng et al., 2020). The target triggers a conformational change of two probes labeled with a redox reported and the change of the signal intensity is monitored to confirm the presence of the target. The approaches above all rely on voltammetric

measurements, require electrode modifications and are complex, thus the need for an alternative, easy-to-use methodology is evident.

Here we propose the use of singlet oxygen ($^1O_2$)-based photoelectrochemistry for the detection of several single-point mutations in the *KRAS* oncogene. This strategy offers several significant improvements compared to existing electrochemical technologies since it relies on an amperometric readout which is easy to interpret, does not require enzymes or electrode modifications, is fast and is easy to use. The detection paradigm is based on the reliability of photoelectrochemical detection combined with catalytic signal amplification by a robust chemical type II photosensitizer molecule, that needs only air and light to produce $^1O_2$, and was proposed by De Wael and coworkers (Trashin et al., 2017). The analytical signal or response, i.e. photocurrent, is triggered only by light and it can thus be clearly distinguished from the background (e.g. buffer, plasma) by simply switching the light off, which is a unique beneficial feature of our photoelectrochemical methodology. Recently, Shanmugam et al. studied a series of photosensitizer-labeled DNA probes in a duplex assay to assess their ability to generate a photocurrent upon illumination with a diode laser (Shanmugam et al., 2022). They found that the sensitivity of the assay increases in the presence of a redox reporter, i.e. hydroquinone, and when the probes are captured at the surface of magnetic beads instead of being directly immobilized at the electrode surface or probes free in solution.

In this study, we have taken the $^1O_2$-based photoelectrochemical strategy to new heights, expanding its capabilities to detect single-point mutations. Specifically, we have focused on the detection of three distinct and clinically relevant *KRAS* hotspot mutations: *i) KRAS* p.G12C (c.34G>T), *ii) KRAS* p.G13D (c.38G>A), and *iii) KRAS* p.Q61H (c.183A>C). To avoid cross-reactivity with closely related sequences, especially their wild-type sequences, which only differ by one nucleotide, the analysis was established at the optimal hybridization temperature. Additionally, the analytical performance (i.e. limit of detection (LOD), sensitivity and linear range) of the photoelectrochemical detection strategy was determined. Finally, the specificity was investigated by performing *KRAS* mutation detection in the presence of genomic DNA of human origin. We show that our approach is highly specific and rapid, while it does not require electrode modifications or the use of enzymes, pushing the boundaries of molecular analysis and opening doors to precision diagnostics.

2. MATERIAL AND METHODS

2.1. Reagents and DNA sequences

Trizma® hydrochloride (Tris HCl), potassium phosphate monobasic salt, Tween-20 and Titriplex® III (ethylenedinitrilotetraacetic acid disodium salt dihydrate, EDTA) were purchased at Merck (Germany), sodium chloride and dimethyl sulfoxide (DMSO) were acquired from Thermo Fisher Scientific (USA), potassium chloride was obtained from Union Chimique Belge (Belgium) and chlorin e6 (purity ≥ 98%) was acquired from Cayman Chemical Company (USA).

The DNA probes were designed to ensure specificity for the *KRAS* mutation of interest and this was verified using the Nucleotide Basic Local Alignment Search Tool. Additionally, the capture probe was designed to recognize the single nucleotide mutation in the middle of the probe. All DNA sequences (Table 2) were synthesized, modified and purified by Eurogentec (Belgium). Capture probes were modified with biotin via a triethylene glycol (TEG) spacer and detection probes were labeled with chlorin e6 via an amino C6 linker. The DNA sequences were solubilized in doubly deionized water (18.2 MΩ cm^{-1}, Arium® Mini, Sartorius, Germany) and the concentration of all DNA sequences was verified using a NanoPhotometer N60 (Implen, Germany) using extinction coefficients calculated based on the sequences by the software. The probes were aliquoted, stored at -20°C and freeze-thaw cycles were avoided to ensure their stability.

The hybridization buffer contained 5 mM Tris HCl, 0.5 mM EDTA and 1 M sodium chloride at pH 7.5 with 0.1% v/v Tween-20, unless specified otherwise. The measuring buffer contained 0.1 M potassium chloride and 0.01 M potassium phosphate monobasic at pH 7. Both buffers were prepared using doubly deionized water. The pH was measured using a pH meter (914 pH/Conductometer, Metrohm, Switzerland). A 15 mM stock solution of hydroquinone (Acros Organics, Belgium) was prepared in measuring buffer.

The human prostate cancer cell line, PC-3, was obtained from the Translational Cancer Research Unit (TCRU) and cultured according to the standard protocols from the American Type Culture Collection (ATCC) (American Type Culture Collection, n.d.). Genomic DNA was extracted using the Blood & Cell Culture DNA Maxi Kit (Qiagen, Germany) according to the manufacturer's guidelines. Using the M220 Focused-ultrasonicator™ (Covaris Inc., USA) DNA was sheared into fragments of approximately 200 base pairs and stored at -20°C.

Table 2. **Sequences and respective modifications for each of the oligonucleotides used to detect *KRAS* mutations (p.G12C, p.G13D and p.Q61H) using the photoelectrochemical methodology.** Part of the target complementary to the capture and detection probe are represented in orange and green, respectively. The single-point mutations in the target are indicated in red. TEG = triethylene glycol spacer.

Name	5' modification	Sequence (5' → 3')	3' modification
p.G12C Capture		CTACGCCACAAGCTCCA	Biotin-TEG
p.G12C Target		TGGAGCTTGTGGCGTAGGCAAGAGTGCCTTGACG	
p.G12C Target WT		TGGAGCTGGTGGCGTAGGCAAGAGTGCCTTGACG	
p.G12C Detection	Chlorin e6	CGTCAAGGCACTCTTGC	
p.G13D Capture		GCCTACGTCACCAGCTC	Biotin-TEG
p.G13D Target		GAGCTGGTGACGTAGGCAAGAGTGCCTTGACGATAC	
p.G13D Target WT		GAGCTGGTGGCGTAGGCAAGAGTGCCTTGACGATAC	
p.G13D Detection	Chlorin e6	GTATCGTCAAGGCACTCTT	
p.Q61H Capture		GTACTCCTCGTGACCTGC	Biotin-TEG
p.Q61H Target		GCAGGTCACGAGGAGTACAGTGCAATGAGGGACCA	
p.Q61H Target WT		GCAGGTCAAGAGGAGTACAGTGCAATGAGGGACCA	
p.Q61H Detection	Chlorin e6	TGGTCCCTCATTGCACT	
Random target		GTATCTATATTCATCATAGGAAACACCAAAGATGATA	

2.2. DNA immobilization and hybridization

A fraction of 10 µL streptavidin-coated magnetic beads (Dynabeads M-280 Streptavidin, 10 mg/mL, Invitrogen by Thermo Fisher Scientific, USA) was loaded in a DNA LoBind® tube (Eppendorf, Germany), vortexed and washed three times using 1 mL of hybridization buffer. After removing the buffer, biotinylated capture probes (48 nM, 1 mL) were added to the magnetic beads using reverse pipetting and the mixture was vortexed and incubated for 15 minutes in a hybridization oven (15 rpm at room temperature, UVP Hybridizer Oven, Analytik Jena, USA). After quickly spinning down the tubes using a mini-centrifuge, the magnetic beads were washed with 1 mL of hybridization buffer and the remaining buffer was removed. Next, a 1 mL mixture of target DNA (24 nM, unless specified otherwise) and photosensitizer-labeled detection probes (24 nM) was added using reverse pipetting. For the experiments with human genomic DNA, the PC-3 cell-line DNA was denatured at 90°C before being added to the mixture of target and detection probe to reach a final concentration of 20 ng/mL. The mixture was vortexed and incubated for 10 minutes in the hybridization oven (15 rpm at a temperature specified throughout the manuscript). After incubation, the tubes were quickly transferred into a water bath, at the same temperature as in the hybridization oven. Finally, the magnetic beads were washed three times using 1 mL of hybridization buffer and stored at room temperature in the dark before the measurements. The entire sample preparation takes less than one hour and a schematic representation of the protocol is shown in Supplementary Figure 1.

2.3. Photoelectrochemical measurements

The photoelectrochemical measurements were performed on a PalmSens4 potentiostat (PalmSens, The Netherlands) and controlled using PSTrace 5.9 software (PalmSens, The Netherlands). A 660 nm light-emitting diode (LED) within a pE-4000 illumination system (CoolLED, United Kingdom) was used to illuminate the electrode surface. The power was adjusted to 30 mW using a PM100D Optical Power Meter (ThorLabs, Inc., USA). The on/off switch for illumination was preprogrammed and controlled using the digital I/O lines present in the PSTrace 5.9 software. Optically transparent gold-sputtered electrodes (AUTR10, DropSens, Spain) containing a carbon auxiliary electrode and a silver pseudo-reference electrode were used for all measurements. Before the measurements, the magnetic beads were resuspended in 10 µL of measuring buffer with 1 mM hydroquinone and gently transferred into the measuring drop (100 µL of measuring buffer with 1 mM hydroquinone). By placing a neodymium magnet underneath the working electrode, all magnetic beads precipitated quickly onto the electrode. All light-chopped chronoamperometry (light 60 s off, 10 s on, 30 s off) experiments were carried out at a constant potential of -0.20 V vs. pseudo reference electrode.

2.4. Data analysis

Data analysis of all chronoamperometric curves was performed using a custom MATLAB R2022a script with the 'findpeaks' function (MathWorks, n.d.) allowing peak identification. The minimum of each peak current was subtracted by the baseline which is determined as the average of the 10 sample points, i.e. 1 second, before illumination. To aid data interpretation, the baseline of the presented raw chronoamperometric data is moved to 0 µA using the linear baseline correction contained within the PSTrace 5.9 software. The represented photocurrents are the average of at least three samples with the standard deviation (n = 3). The discrimination efficiency and its error were calculated using Equation (1) and Equation (2), respectively, in which I_{WT} is the photocurrent of the wild-type target, I_{Mut} the photocurrent of the mutation target, and σ the standard deviation.

$$Discrimination\ efficiency = \left(1 - \frac{I_{WT}}{I_{Mut}}\right) \cdot 100 \qquad (1)$$

$$Error\ on\ discrimination\ efficiency = \left(\frac{I_{WT}}{I_{Mut}} \sqrt{\left(\frac{\sigma_{I_{WT}}}{I_{WT}}\right)^2 + \left(\frac{\sigma_{I_{Mut}}}{I_{Mut}}\right)^2}\right) \cdot 100 \qquad (2)$$

The LOD was determined using Equation (3) in which σ_{Blank} is the standard deviation of the photocurrent without the target present (n = 3) and a is the slope of the obtained calibration plot.

$$LOD = \frac{3.3 \cdot \sigma_{Blank}}{a} \qquad (3)$$

3. RESULTS AND DISCUSSION

The working principle of the photoelectrochemical approach to detect single-point mutations is illustrated in Figure 1. The part of the target sequences containing the mutation (blue) is complementary to an oligonucleotide, named capture probe (orange). This capture probe is labeled with biotin to allow immobilization on streptavidin-coated magnetic beads via a biotin-streptavidin interaction. These beads are concentrated on the working electrode surface using a magnet positioned below the electrode. The detection probe (green) is labeled with a type II photosensitizer and complements another part of the target of interest. This type II photosensitizer is excited upon illumination, undergoes intersystem crossing and then transfers its energy to molecular oxygen to generate $^1O_2$ (Nonell and Flors, 2016). Chlorin e6 was chosen as a photosensitizer since it has a high $^1O_2$ quantum yield and can be easily coupled to DNA (Redmond and Gamlin, 1999). In the presence of the target, a so-called sandwich hybrid is formed. Upon illumination of the sandwich hybrid, captured at the electrode, using an LED, $^1O_2$ is produced by the photosensitizer (Nonell and Flors, 2016). $^1O_2$ acts as a strong oxidant and oxidizes the redox reporter present in the measuring solution, i.e. hydroquinone (Trashin et al., 2017), forming benzoquinone. This oxidation process is followed by electrochemical regeneration of the redox reporter at the electrode surface by applying the correct potential. This completes the electrocatalytic redox cycle resulting in an amplified photoelectrochemical response, named photocurrent. Importantly, $^1O_2$ is produced in a controlled way by a short illumination of 10 s and a rapid reaction with the redox reporter hydroquinone to avoid oxidative damage to the DNA probes. Ultimately, when the target is absent, the sandwich hybrid is not formed and, as a result, the photosensitizer-labeled detection is washed away and no photocurrent is recorded.

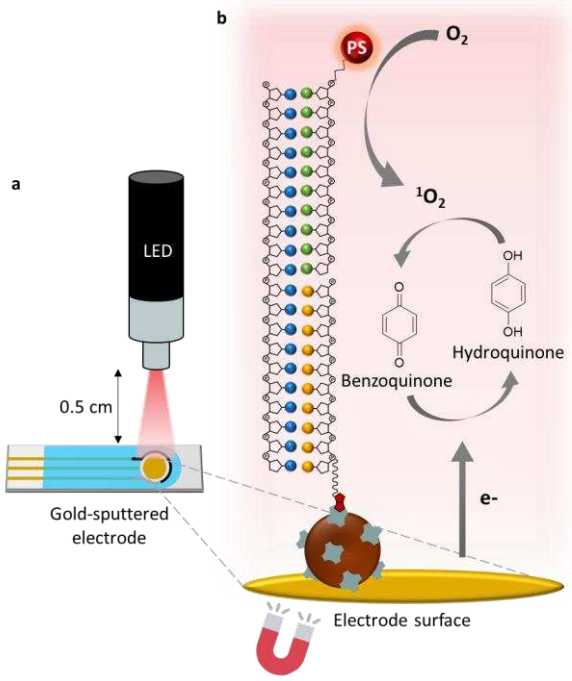

Figure 1. **The $^1O_2$-based photoelectrochemical detection principle.** Schematic representation of detection principle for single-point mutations with **a)** a top view of the gold-sputtered electrode with the LED source and **b)** a zoom on the electrode surface. The sandwich hybrid consists of a biotin-labeled capture probe (orange), target sequence (blue) and photosensitizer-labeled detection probe (green). The capture probe is coupled to a magnetic bead which is in turn attracted to the working electrode surface using a magnet.

3.1. Enhancing specificity by using the optimal hybridization temperature

The capture and detection probes are designed to be fully complementary to the target DNA sequence with mutation, but undesired reactions with other closely related DNA sequences can interfere. Especially the wild type, which only differs by one nucleotide, can non-specifically bind to the capture probe and contribute to the photocurrent response. To mitigate such undesired interactions, hybridization needs to be optimized (Zhang et al., 2012). By performing the reaction at the optimal hybridization temperature, the stringency increases, only enabling specific hybridization of the target of interest. For the *KRAS* p.G12C mutation, a temperature screening was performed to determine the optimal hybridization temperature. The range between 62°C and 71°C was selected based on the theoretical melting temperature of the target and capture probe, i.e. 65.0°C, as determined using the OligoAnalyzer™ Tool of Integrated DNA Technologies (Supplementary Table 2). Figure 2a and Supplementary Figure 2 show that the photocurrents of both the *KRAS* p.G12C target (24 nM) and wild type (24 nM) are gradually decreasing when increasing the temperature, from -2.9 ± 0.1 µA to -0.20 ± 0.05

µA and -1.48 ± 0.06 µA to -0.141 ± 0.005 µA, respectively. This indicates that fewer sandwich hybrids are formed at higher temperatures. In addition, the photocurrent of the wild type reaches a minimum around 67°C, while the photocurrent of the *KRAS* p.G12C target keeps on decreasing until the highest temperature studied (71°C). This can be explained by the full complementarity of the *KRAS* p.G12C target to the capture and detection probe while the wild type contains a single mismatch that destabilizes the sandwich hybrid. When no target is present, a low background photocurrent is observed which increases slightly at higher temperatures (maximum -0.020 ± 0.002 µA).

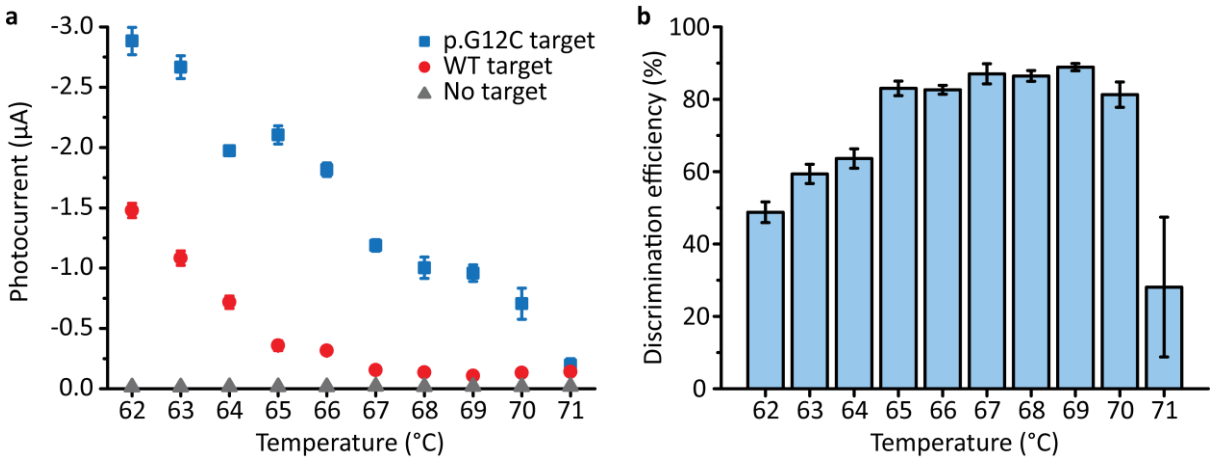

Figure 2. **Temperature screening of the *KRAS* p.G12C target. a)** Average photocurrent recorded for *KRAS* p.G12C target (blue), wild-type (WT) target (red), and no target (gray) after hybridization of probes and target was performed at various temperatures (62-71°C) in hybridization buffer with 0.05% of Tween-20. **b)** Discrimination efficiency between the *KRAS* p.G12C and wild-type targets.

The optimal hybridization temperature is defined as the temperature at which the ratio of photocurrent between the mutation and wild type is the highest, represented by the discrimination efficiency (Figure 2b). At the lowest temperature studied (62°C), the discrimination efficiency is 49 ± 3% and this gradually increases until 87 ± 3% at 67°C. At higher temperatures, the discrimination efficiency decreases again until the discrimination becomes inaccurate at 71°C (28 ± 19%). At 69°C, the discrimination efficiency is slightly higher (89 ± 1%) than at 67°C, due to the very low photocurrent of the wild-type target (-0.107 ± 005 µA). However, since the background photocurrent (no target) increases at higher temperatures, we selected 67°C as the optimal hybridization temperature. The contribution of the photocurrent in the absence of a target is most probably due to non-specific adsorption of the photosensitizer-labeled detection probe to the magnetic beads (Wang et al., 1998). Therefore, the concentration of Tween-20 in the hybridization buffer was increased to 0.1%

for further experiments without losing sensitivity for the *KRAS* p.G12C target (Supplementary Figure 3). The optimal hybridization temperature for the *KRAS* p.G13D and *KRAS* p.Q61H targets was determined in a similar fashion and set to 68°C and 67°C, respectively (Supplementary Figure 4).

Negative control tests in which the target or one of the probes is absent were performed at the optimal hybridization temperature, i.e. 67°C for the *KRAS* p.G12C mutation (Figure 3a and b). When the target or one of the probes, i.e. capture probe or detection probe, is absent the photocurrent is negligible ($< 0.080 \pm 0.002$ µA). The use of an elevated temperature during hybridization of the target with the probes is crucial to detect a single-point mutation specifically via photoelectrochemistry, allowing to distinguish between mutation and wild-type targets. Performing the experiments at 25°C results in a more intense signal for the wild-type target since the sandwich hybrid with this target is stable at lower temperatures (Figure 3c and d). However, removing one of the sequences in the sandwich hybrid did not result in a noticeable photocurrent indicating that all components are crucial to obtain a response.

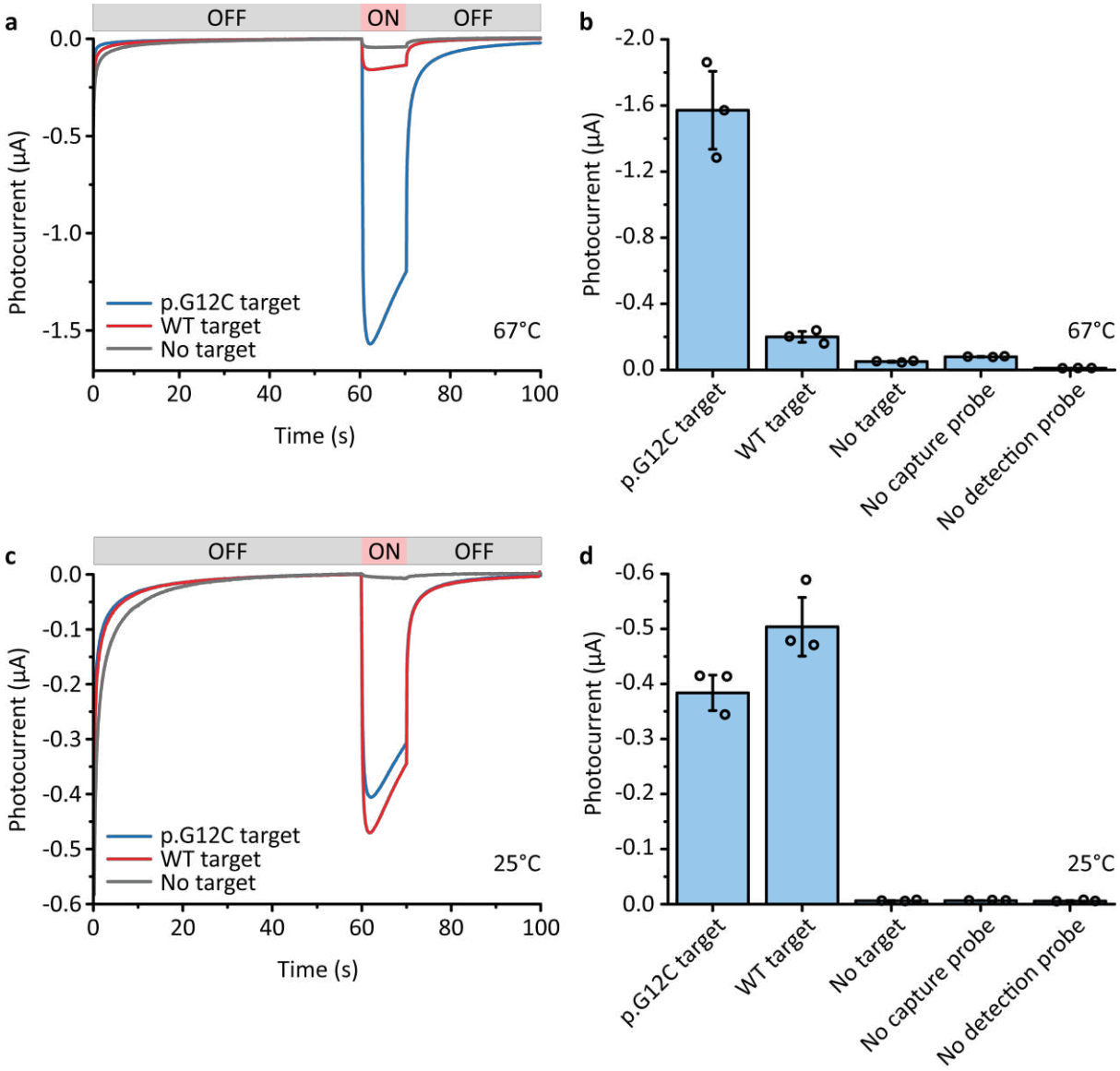

Figure 3. **Effect of the hybridization temperature and negative controls.** Chronoamperometric data for *KRAS* p.G12C target (blue), wild-type (WT) target (red), and no target (gray) after hybridization of probes and target was performed at **a)** 67°C or **c)** 25°C in hybridization buffer with 0.1% of Tween-20. Corresponding photocurrents were recorded at **b)** 67°C or **d)** 25°C.

The use of the optimal hybridization temperature causes an increase in the photocurrent intensity. This is most prominent for the *KRAS* p.G12C target in which the photocurrent changes from -0.38 ± 0.03 µA at 25°C to -1.6 ± 0.2 µA at 67°C. This effect is most likely due to secondary structure formation of the target at 25°C which hampers the binding to the probes and, thus, lowers the signal.

Negative control experiments were also performed for the *KRAS* p.G13D and p.Q61H targets (Supplementary Figure 5) at their optimal hybridization temperature. Once again, there is a clear distinction between the *KRAS* and wild-type targets with a discrimination efficiency of 84 ± 5% and 93.9 ± 0.8% for *KRAS* p.G13D and p.Q61H, respectively. The difference in discrimination efficiency for the *KRAS* mutations can be explained by the difference in melting temperature of their mutation and wild-type targets (Supplementary Table 2). The *KRAS* p.G13D mutation has the smallest difference in melting temperature, i.e. 2.9°C, which results in the lowest discrimination efficiency (84 ± 5%) since the temperature range to distinguish between mutation and wild-type targets is very narrow. In contrast, the *KRAS* p.Q61H mutation has a difference in melting temperature between the mutation and wild-type target of 6.6°C, resulting in a high discrimination efficiency of 93.9 ± 0.8%. The *KRAS* p.G12C mutation has an intermediate difference in melting temperatures of 5.2°C which results in a discrimination efficiency of 87 ± 3%. Differences in melting temperature between the mutation and wild-type sequences are attributed to differences in base pair and mismatch stability as described by SantaLucia and Hicks (SantaLucia and Hicks, 2004).

3.2. Determining the analytical performance of the photoelectrochemical methodology

In the next step, the analytical performance of the photoelectrochemical methodology was determined for the *KRAS* p.G12C target (Figure 4a and Supplementary Figure 6). A calibration plot in the target concentration ranging from 38 pM to 24 nM (five-fold dilutions) was constructed in hybridization buffer and in the same buffer with human genomic DNA that did not contain the mutation of interest. The concentration of human genomic DNA was set to 20 ng/mL to mimic the concentration of cell-free DNA in a liquid biopsy sample (i.e. plasma) (Beckman Coulter, 2022; Boons et al., 2022). The LOD in hybridization buffer was calculated to be 117 pM (1.24 ng/mL), while the LOD in the presence of human genomic DNA was 145 pM (1.54 ng/mL) in the range 192 pM – 24 nM. Importantly, there is a linear trend between the photocurrent and concentration (Supplementary Figure 6) with a linear range between 355 pM – 24 nM in buffer and 440 pM – 24 nM in the presence of human genomic DNA, indicating that the methodology can be employed for the quantification of cancer biomarkers. Within this range, the sensitivity, i.e. the change in photocurrent per change in concentration, was determined to be 75 nA/nM^{-1} in hybridization buffer and 38 nA/nM^{-1} in the presence of human genomic DNA. As a control, a random DNA sequence (Table 2) was measured and no significant photocurrent was observed, showing that there is no non-specific binding occurring. The photocurrent of the *KRAS* p.G12C target decreased two-fold in the presence of human genomic DNA compared to pure buffer most likely due to matrix effects that hamper the hybridization of the *KRAS* p.G12C target to the capture and detection probes (Figure 4b).

However, when no target was added, the human genomic DNA itself did not show a response which is an additional indication there is no non-specific binding.

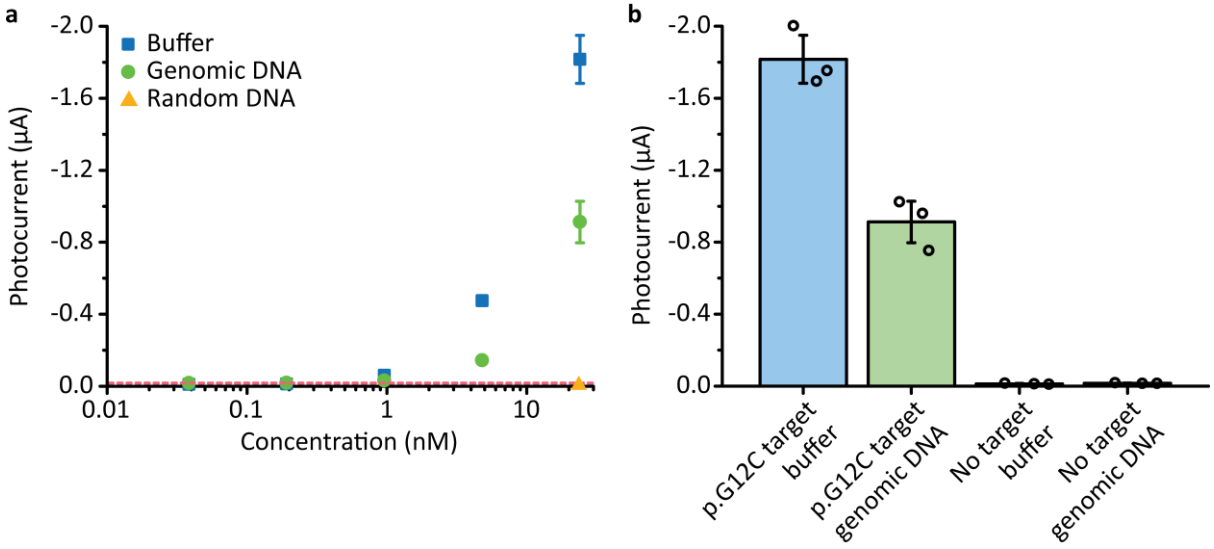

Figure 4. **Chronoamperometric detection of the *KRAS* p.G12C target in buffer and human genomic DNA. a)** Calibration plot of the *KRAS* p.G12C target (3.84 pM – 24 nM, five-fold dilutions) in hybridization buffer with 0.1% of Tween-20 (blue) and in the same buffer in which human genomic DNA was added (green). The photocurrent of the sample without a target is represented by the pink dashed line and the photocurrent of 24 nM of a random DNA target is represented by an orange triangle. **b)** Photocurrent of the *KRAS* p.G12C target or no target in hybridization buffer with 0.1% of Tween-20 (blue) and in the same buffer in which human genomic DNA was added (green).

Finally, a calibration plot was constructed for the *KRAS* p.G13D and p.Q61H mutations (Supplementary Figure 7). For the *KRAS* p.G13D target, the LOD was calculated to be 112 pM (1.25 ng/mL) and 272 pM (3.04 ng/mL) in hybridization buffer and in the presence of human genomic DNA, respectively. The LOD of the *KRAS* p.Q61H target was determined to be 117 pM (1.28 ng/mL) in both conditions. Once again, a linear relationship between the photocurrent and concentration was observed with a linear range of 339 pM – 24 nM in hybridization buffer and 825 pM – 24 nM with human genomic DNA present for the *KRAS* p.G13D target, and 355 pM – 24 nM and 355 pM – 24 nM for the *KRAS* p.Q61H target in hybridization buffer and in the presence of human genomic DNA, respectively. For both mutations, the photocurrent of the random DNA sequence was negligible (-0.029 ± 0.004 µA for *KRAS* p.G13D and -0.038 ± 0.005 µA for *KRAS* p.Q61H). These photocurrents are comparable to the photocurrent without a target present (-0.027 ± 0.001 µA and -0.034 ± 0.002 µA for *KRAS* p.G13D and p.Q61H, respectively) showcasing that no non-specific binding takes place. Ultimately, the LOD of all

mutations is comparable (117 pM, 112 pM and 117 pM for *KRAS* p.G12C, p.G13D and p.Q61H, respectively) and provides a clear image of the LOD of the $^1O_2$-based methodology in buffer solutions. In the presence of human genomic DNA, the LOD varies slightly (145 pM, 272 pM and 117 pM for *KRAS* p.G12C, p.G13D and p.Q61H, respectively) which could be explained due to matrix effects in which the hybridization of the target and probes is influenced during the sample preparation.

4. CONCLUSIONS

This work describes the development of a novel $^1O_2$-based photoelectrochemical strategy for detecting specific single-point mutations in the *KRAS* oncogene. The optimal temperature to perform the hybridization of the sandwich hybrid was determined. By performing the hybridization at the optimal temperature, we were able to specifically detect a single-point mutation and discriminate this from its wild-type sequence. Furthermore, the specificity of the methodology was proved by performing experiments in the presence of a random DNA sequence and human genomic DNA which did not contain the *KRAS* mutation of interest. Afterwards, the LOD of the methodology was calculated to be between 112 and 117 pM (1.25 ng/mL – 1.28 ng/mL) in buffer and between 117 and 272 pM (1.28 ng/mL – 3.04 ng/mL) in the presence of human genomic DNA, without the need for additional PCR or other amplification techniques. However, for real-life applications, the signal of the wild-type targets should be considered as a threshold to determine the sensitivity of the methodology. While the obtained LOD is not yet sufficient to detect clinically relevant levels of cancer biomarkers, this work provides a proof of concept for the detection of single-point mutations using the $^1O_2$-based photoelectrochemical methodology. In the future, a biotechnological approach can be integrated to amplify the signal and thus boost the sensitivity. A target amplification-free technology would avoid PCR duplicates and reduce contamination risks in the clinic. Moreover, the methodology itself, e.g. the illumination power, can be further optimized to enhance sensitivity. In order to translate the $^1O_2$-based photoelectrochemical methodology to clinical samples, further steps need to be taken in terms of e.g. investigating the effect of double-stranded DNA. Additionally, developing the methodology to detect multiple biomarkers, e.g. the three KRAS mutations, simultaneously will be explored in the future.

To conclude, the $^1O_2$-based photoelectrochemical methodology can be easily expanded towards other biomarker sequences (e.g. any disease needing mutation detection) and types (e.g. RNA) by redesigning the capture and detection probes and determining their optimal hybridization temperature. Additionally, thanks to the decoupling of the DNA handling from the photoelectrochemical detection using magnetic beads, the detection technology has the

potential to be applied in a lot of different matrices (e.g. in germline DNA, in cell-free DNA, and in plasma). Ultimately, the photoelectrochemical strategy has unique features compared to other methodologies, such as being rapid with an analysis time below two minutes, affordable, highly specific and easy to use since only few components are required (i.e. no enzymes) and electrodes should not be modified. This showcases the potential of this methodology in nucleic acid-based diagnostics.

ACKNOWLEDGEMENTS

This work was supported by the Fund for Scientific Research (FWO) Flanders [grant numbers G078223N, G054819N, 1S39323N to S.B., 1S94923N to L.M. and 1803723N to T.V.]; and the Bijzonder Onderzoeksfonds [grant numbers iBOF/23/030, BOF SEP K.D.W].

AUTHOR CONTRIBUTIONS

Elise Daems: Conceptualization, Data Curation, Investigation, Methodology, Validation, Visualization, Writing - Original Draft, Writing - Review & Editing. Simone Bassini: Conceptualization, Data Curation, Formal analysis, Investigation, Methodology, Validation, Visualization, Writing - Original Draft, Writing - Review & Editing. Laura Mariën: Investigation, Writing - Review & Editing. Hannah Op de Beeck: Data Curation, Investigation, Software, Writing - Review & Editing. Alexandr Stratulat: Writing - Review & Editing. Timon Vandamme: Writing - Review & Editing. Karen Zwaenepoel: Writing - Review & Editing. Ken Op de Beeck: Resources, Supervision, Writing - Review & Editing. Senada Koljenovic: Funding acquisition, Writing - Review & Editing. Marc Peeters: Funding acquisition, Writing - Review & Editing. Guy Van Camp: Funding acquisition, Resources, Supervision, Writing - Review & Editing. Karolien De Wael: Conceptualization, Methodology, Funding acquisition, Project administration, Resources, Supervision, Writing - Review & Editing.

COMPETING INTERESTS

The authors declare that they have no known competing financial interests or personal relationships that could have appeared to influence the work reported in this paper.

DATA AVAILABILITY

Data will be made available on reasonable request.

REFERENCES

American Type Culture Collection, n.d. PC-3. https://www.atcc.org/products/crl-1435#detailed-product-information (accessed 7.19.23).

Attoye, B., Baker, M.J., Thomson, F., Pou, C., Corrigan, D.K., 2021. Biosensors 11, 42.

Attoye, B., Pou, C., Blair, E., Rinaldi, C., Thomson, F., Baker, M.J., Corrigan, D.K., 2020. Biosensors 10, 156.

Beckman Coulter, 2022. Comparative analysis of cell-free DNA extra efficiency from plasma.

Boons, G., Vandamme, T., Mariën, L., Lybaert, W., Roeyen, G., Rondou, T., Papadimitriou, K., Janssens, K., Op de Beeck, B., Simoens, M., Demey, W., Dero, I., Van Camp, G., Peeters, M., Op de Beeck, K., 2022. Clin. Cancer Res. 28, 338–349.

Das, J., Ivanov, I., Montermini, L., Rak, J., Sargent, E.H., Kelley, S.O., 2015. Nat. Chem. 7, 569–575.

Global Cancer Observatory, 2020. https://gco.iarc.fr/today/home.

Heller, A., Feldman, B., 2008. Chem. Rev. 108, 2482–2505.

Hong, D.S., Fakih, M.G., Strickler, J.H., Desai, J., Durm, G.A., Shapiro, G.I., Falchook, G.S., Price, T.J., Sacher, A., Denlinger, C.S., Bang, Y.-J., Dy, G.K., Krauss, J.C., Kuboki, Y., Kuo, J.C., Coveler, A.L., Park, K., Kim, T.W., Barlesi, F., Munster, P.N., Ramalingam, S.S., Burns, T.F., Meric-Bernstam, F., Henary, H., Ngang, J., Ngarmchamnanrith, G., Kim, J., Houk, B.E., Canon, J., Lipford, J.R., Friberg, G., Lito, P., Govindan, R., Li, B.T., 2020. New Engl. J. Med. 383, 1207–1217.

Kimmel, D.W., LeBlanc, G., Meschievitz, M.E., Cliffel, D.E., 2012. Anal. Chem. 84, 685–707.

Lee, S., You, J., Baek, I., Park, H., Jang, K., Park, C., Na, S., 2022. Biosens. Bioelectron. 210, 114295.

MathWorks, n.d. findpeaks function. https://nl.mathworks.com/help/signal/ref/findpeaks.html (accessed 9.11.23).

Nonell, S., Flors, C., 2016. Singlet Oxygen: Applications in Biosciences and Nanosciences. Royal Society of Chemistry.

Ondraskova, K., Sebuyoya, R., Moranova, L., Holcakova, J., Vonka, P., Hrstka, R., Bartosik, M., 2023. Anal. Bioanal. Chem. 415, 1065–1085.

Redmond, R.W., Gamlin, J.N., 1999. Photochem. Photobiol. 70, 391–475.

SantaLucia, J., Hicks, D., 2004. Annu. Rev. Biophys. Biomol. Struct. 33, 415–440.

Shanmugam, S.T., Trashin, S., De Wael, K., 2022. Biosens. Bioelectron. 195, 113652.

Sholl, L.M., Halmos, B., 2022. Br. J. Cancer 127, 1177–1179.

Trashin, S., Rahemi, V., Ramji, K., Neven, L., Gorun, S.M., De Wael, K., 2017. Nat. Commun. 8, 16108.

Vacante, M., Borzì, A.M., Basile, F., Biondi, A., 2018. World J. Clin. Cases 6, 869–881.

Wang, H.-F., Ma, R.-N., Sun, F., Jia, L.-P., Zhang, W., Shang, L., Xue, Q.-W., Jia, W.-L., Wang, H.-S., 2018. Biosens. Bioelectron. 122, 224–230.

Wang, J., Rivas, G., Fernandes, J.R., Lopez Paz, J.L., Jiang, M., Waymire, R., 1998. Anal. Chim. Acta 375, 197–203.

Weinberg, R.A., 1996. Sci. Am. 275, 62–70.

Yuanfeng, P., Ruiyi, L., Xiulan, S., Guangli, W., Zaijun, L., 2020. Anal. Chim. Acta 1121, 17–25.

Zeng, N., Xiang, J., 2019. Talanta 198, 111–117.

Zhang, D.Y., Chen, S.X., Yin, P., 2012. Nat. Chem. 4, 208–214.

Zhou, X., Liu, X., Xia, X., Yang, X., Xiang, H., 2020. J. Electroanal. Chem. 870, 114270.